The study of the electron transport characteristics of bilayer blue phosphorus with different stacking by first principles

Si-Cong Zhu, [1, 2, a)] Shun-Jin Peng, [1] Kai-Ming Wu,[1] Cho-Tung Yip, [3] Shu-Ling Wang,[2,4] Kai-Lun Yao[5] and Chi-Hang Lam[2,b)]

[1]College of Science and Key Laboratory for Ferrous Metallurgy and Resources Utilization of Ministry of Education, Wuhan University of Science and Technology, Wuhan 430065, China

[2]Department of Applied Physics, Hong Kong Polytechnic University, Hung Hom, Hong Kong, China

[3] Department of Physics, Shenzhen Graduate School, Harbin Institute of Technology, Shenzhen 518055, China

[4]School of Mathematics and Physics, Hebei University of Engineering, Handan 056038, China.

[5]Wuhan National High Magnetic Field Center and School of Physics, Huazhong University of Science and Technology, Wuhan 430074, China

[a)]Electronic address: sczhu@wust.edu.com

[b)]Electronic address: C.H.Lam@polyu.edu.hk

Abstract

We study the structural, electronic and transport property of bilayer blue phosphorus by using the first-principles. Our results show that the band gap can be adjusted by different stacking structures of the bilayer blue phosphorus. We simulate the functional device based on AA-, AB- and AC stacking bilayer blue phosphorus and the transport characteristics of the current-voltage curve with nonlinear competitive behavior are investigated. Of the three devices, AA stacking bilayer blue phosphorus has the highest conductivity. Under special bias, the currents of AB- and AC stacking devices produce interesting competitive behavior. The transport characteristics behaviors of the bilayer blue phosphorus can be explained by the band structure, transport spectrum and molecular projected self-consistent Hamiltonian (MPSH). We can control the change of current by adjusting the different contact modes of the bilayer blue phosphorus. The bilayer blue phosphorus with interesting electronic and transport properties are expected to have potential applications in nanoelectronics.

Introduction

Two-dimensional (2D) materials have attracted huge interest and led to a prosperous development in both fundamental and applied studies in various fields [1-5]. Among various 2D semiconductor, due to the unique properties of phosphorene [3-5], such as direct band gap [5, 6] and high carrier mobility (~1000 $cm^2\ V^{-1}s^{-1}$) [3], this new 2D semiconductor has high potential to be the core materials of next generation nanoelectronic devices. The black phosphorus is the most stable phosphorus and layered structure of an elemental solid as graphene. Individual layers of black

phosphorus are nonplanar honeycomb structure.

As the allotrope of black phosphorus, Zhu have studied its stability by first principle methods and found that it can be as stable as black phosphorene [7]. The new two-dimensional material, known as blue phosphorous (BlueP), has a cell of two sublattices that resemble a honeycomb lattice but are not on the same horizontal plane [see figure 1(a)], forming a periodically buckled structure. Unlike zero band gap graphene, BlueP possesses 2.0eV energy gap, which is considerably higher than that of black phosphorus [7, 8]. Recently, Xu and Zhang have successfully grown a single layer of blue phosphorus on the Au(111) membrane by molecular beam epitaxy (MBE) [9,10]. Unlike other two-dimensional materials such as graphene [11] and transition metal dichalcogenides [12], the phosphorus atoms bond with three neighboring phosphorus atoms to form a special, buckled structure. Based on the first principles calculation, a method of modulation the blue band gap by adjusting the number of blue phosphorus layers is proposed [13]. The energy gap is increased when the layers number is decreased. Another way to modulate the physical properties of BlueP is to change the two-layer stack. Two layers of BlueP stacked AA, AB, or AC also have a smaller band gap than a single layer. [19].

In our work, we focus on the electrical property of pure bilayer BlueP by density functional theory calculation (DFT) [14, 15]. We calculate the band structures of different stacked bilayer BlueP and simulate the sandwich devices based on bilayer BlueP. The transport properties are studied through DFT combined with nonequilibrium Green's function (NEGF) [16-18], where atomic relaxations of the whole system are taken into account. We will study AA-, AB- and AC stacking BlueP.

Theory and Methods

The calculations are based on Virtual Atomistix ToolKit (ATK) [16-18]. The DFT calculations of bilayer BlueP are performed with the Perdew-Burke-Ernzerhof (PBE) and generalized gradient approximation (GGA).

In order to expend the electron density, a double-ζ polarized basis set is used. We sample the 12 ×12 × 6 K-points in the Brillouin zone (BZ) of the bilayer BlueP bulks. The maximum force is 0.05 eV $Å^{-1}$ and the density mesh cut-off is 150 Rydberg during geometry optimizations. We also used Local density approximation (LDA) calculation, and got a similar result. We calculate the electronic property of different stacking bilayer blue phosphorus (BBP) as summarized in Figure 1. In order to avoid spurious interactions caused by the periodic boundary conditions, a vacuum region with a thickness of 15Å along the Z direction is introduced. The side view of BBP can be seen in the Figure 1. In this work, we have optimized both the super cell and the lattice to obtain the most stable

atomic positions.

Results and discussion

All structural parameters are listed in Table 1. For AA stacking (Figure 1a) the second layer is exactly above the first one. But for the AB stacking (Figure 1b), the upper layer is shifted along the xy plane relative to the lower layer., For AC stacking (Figure 1c) the upper layer is not only moved along the xy plane but is also rotated relative to the lower layer. The interlayer distances in the bilayer structures are 3.214Å, 3.248Å and 3.262 Å for AA- , AB- and AC stackings, respectively. The AA stacking BBP possesses the shortest distance between layers and the smallest band gap. The lattice constants and binding energy of AA and AB stacking BBP are similar.

Electronic band structures are plotted in Figure 2 for monolayer BlueP as well as for AA, AB and AC stacking BBP. Each energy band in the monolayer is split into two bands due to interactions between the two adjacent layers. Otherwise, the overall shape of the valence band maximum (VBM) and the conduction band minimum (CBM) are hardly changed except for AC stacking BBP compared with monolayer BlueP, but the band gap is decreased to about 1 eV. For bilayer structures, the p orbital enters the original electronic gap region.

The calculated binding energies (E_b) for three types of stacking constructions are summarized in Table 1. From the results, the AB stacking is the most favor stacking structure. For pure BBP, our results are consistent with those of Ghosh et al [19]. In addition, the lattice constant in the plane is stretched by intercalation, but due to the strong covalent bond of intralayer P–P bonds, the length of P-P bonds is almost unchanged. As illustrated in the Figure 3, we calculate the band gap between the conduction and valence bands as summarized in Table 1. The electronic band structure of monolayer BlueP is qualitatively similar for both GGA and LDA based calculations. They give 1.89 eV (GGA) and 1.73 eV (LDA) band gaps. In particular, the value from GGA is in accordance with those reported in the report [7]. Similarly, BBP is also an indirect energy-gap semiconductor, and the energy gap is about 1 eV for all three stacking sequences (AA, AB, and AC) [see Figures. 2(b)–2(d)]. The value of the band gap of BBP is stacking sequence dependent: 0.987 eV for AA-, 1.100 eV for AB-, and 1.055 eV (GGA) for AC stackings, which is 41–47% less than that of monolayer BlueP.

We also plot the alignment of conduction band minimum (CBM) and valence band maximum (VBM) with respect to the Fermi level, as shown in Figure 3(a) while Figure 3(b) show the corresponding crystalline orbitals. It can be seen that VBMs is similar in the three superimposed modes, while the CBMs of AA superimposed BBP is significantly lower than that of AB and AC. Also, the overlap of interlayer crystalline orbitals of CBM is absent in stacked bilayers. The

electronic orbital state is almost located on one layer for AB stacking BBP, suggesting the weaker interlayer interactions in AB stacking BBP.

We study transport structures of the BBP with atomic positions all determined by the geometry optimization without fixing any phosphorus atoms. It is composed of scattering region and left, right electrode contacts as shown in figure 4 (a). We have optimized the sandwich structures. The electron-dependent transport characteristics of these systems are studied by using DFT and NEGF. In our electric transport calculations, the valence orbitals are expanded in a double-ζ plus polarization (DZP) basis set for all atoms. For the electrodes in Brillouin zone, The 1 × 1 × 100 *k*-points mesh is applied and the cut-off energy is set to 150 Ry for the real space grid.

The current is calculated as

$$J_{\sigma} = \int_{\mu_R}^{\mu_L} T_{\sigma}(E,V)[f(E-\mu_L) - f(E-\mu_R)]dE \quad (1)$$

Where μ_L and μ_R are the chemical potentials of the left and the right electrodes, while f is the Fermi-Dirac distribution.

We simulate a device structure as shown in Figure 4(a), where the scattering region is the centre region and the left and right electrodes are semi-infinite BBP. The electronic transport direction is from left to right and along the z direction, the left and right electrodes are all set to room temperature - 300 K. The calculated I-V curves of the AA-, AB- and AC stackings BBP are as shown in Figure 4(b)-(d), respectively. In the bias voltage rang of [0-1.0V], the currents of the three devices are similar (see Figure 4(c)). The current of the AA stacking device grows quickly while the bias voltage is increased further. The current of AC stacking device grows slowest. When the bias voltage is larger than 1.9V, the current of the AC stacking device has suddenly increased and exceeded the AB one.

In order to explain the transport behaviors in Figure 4, we have also studied the transmission spectra dependent bias voltage and energy level which are summarized in Figure 6. For Eq. (1), the current is definition by the integral of the transmission coefficient and Fermi energies within the bias window. We show the transmission spectra of the AA stacking [Figure 5 (a)] that when the bias voltage is in the range from 0 to 1.3V, in the bias window, the transmission spectra of the transmission channel is suppression. So the current in region I is very low. When the bias increases, the peaks of the transmission spectra move towards into the bias window and the current of AA stacking increases rapidly as shown in region II. For the AB stacking device, the current is in the off state in the bias range from 0 to 1.5 V. When the bias voltage increases further, the current is turned on and increases rapidly. The current-off state of the AC stacking device is attained at a bias voltage from 0V to 1.7V. We see a more rapid increase of the current in the AC stacking device for bias beyond 1.7V.

Figure 4(d) shows the transmission coefficients at four particular bias voltages (0V, 1.0V, 1.6V and 2.0V) for the BBP devices. For AA stacking (see Figure 6), only when the bias is 1.6V in the bias window, there is a transmission peak, leading to the increase of the current. Then, when the bias voltage takes the value 2.0V (see Figure 6), the bias window is enlarged by the increase of the bias voltage, due to the total integral area and the corresponding transmission coefficient become larger, which stands for that the corresponding orbital is opened. In the issue, the current in the AA stacking device is increased. As shown in the Figure 6, for AC stacking, there is no transmission peak in the bias window at the 1.6V while some small transmission peaks move into the bias window for the AB one, so the current for AB stacking exceeds that for the AC one. When the bias voltage reaches 2.0V, the transmission coefficient for AC stacking is higher than the AB one, and the current of AC exceeds that of the AB one. When the bias voltage is in the range from 1.0 to 2.0V, there is an interesting competitive relationship between the currents of AB and AC stacking devices.

As mentioned above, the behaviors of the currents can be explained based on the transmission spectra. And, the origin of the transmission spectra should be correlated with the electron transmission form left to right electrode and will be discussed later. It has been reported that the transmission channel is either open when the symmetries of electronic subbands of the left and right electrodes matches, or closed while the energy levels of left and right electrodes are mismatched at the same energy region [20, 21].

To understand the transmission spectra, we take two particular bias voltages for 1.6 V and 2.0 V and three bilayer configurations (AA, AB and AC) for further study. Figure 7 shows the transmission coefficient (middle panel) and band structures of the left electrode (left panel) and right electrode (right panel) at different bias voltages. When the bias is applicable to left and right electrodes, a positive bias shifts the energy bands up, meanwhile, a negative bias shifts the energy bands down. This leads to a change in the symmetrical matching of the left and right electrodes. Due to the buckling and bilayer structures of BlueP, we cannot find any simple π or σ bonds or antibonds close to the Fermi level. The grey shadow represents the efficacious transmission channel within the bias window (light-grey), which has a significant impact on the electronic transmission, and the grey region denotes that the channel is open for electron flow. Thereupon, from Figure 7, the results show that the voltage-current curve and transmission spectrum of the electrodes are in good agreement with the symmetry of the electrode' band structures.

For AA stacking structure, at bias voltage of 1.6 V (as shown in Figure 7(a)), the *xz* plane mirror symmetry operation relates the Lowest Unoccupied Molecular Orbital (LUMO)-1 of the left electrode(LUMO-1(L)) and the Highest Occupied Molecular Orbital (HOMO) of right electrode(HOMO(R)). Due to the symmetrical matching of the left and right electrodes, the

channel opens within the energy range of [0.05-0.35eV] in the dark gray region, while the channel closes in the rest of the bias window due to the symmetry mismatch.The symmetry matched region of LUMO-1(L) and HOMO(R) is large, leading to the increase of the current in Figure 7(b).

In AB stacking configuration, only the LUMO-1(L) and HOMO(R) have the same symmetry under the Y axis. Similar to AA stacking, the down-shifted LUMO-1(L) matches the up-shifted HOMO(R) and a wider region in the transmission spectra contribute to the current by increasing the bias voltage.

In AC stacking configuration (as shown in the Figure 7(e)), there is no transmission spectrum in the bias window because of the different symmetries of LUMO-1(L) and LUMO (L) compared with the HOMO(R). However, when the bias is 2.0V, the LUMO-2(L) and LUMO -3(L) which are of the same symmetry with the HOMO(R) enters the bias window, causing higher transmission than the AB one. Therefore, the current of AC stacking exceeds that of the AB one at large bias voltage.

Summary

In summary, we have systematically investigated the structural and electronic characters of AA-, AB- and AC stacking bilayer blue phosphorus by means of DFT. We have also demonstrated the nonlinear current behavior of different bilayer blue phosphorus by first principles calculations based on DFT combined with NEGF technique. We construct device structures by sandwiching the BBP with the 2D stacking BBP electrodes and different stacking show different conductivity. The AA stacking bilayer blue phosphorus possesses the best conductivity due to the smallest band gap. Because of the symmetry of the electronic subbands, the current of either AC- or AB stacking BBP can be larger depending on the bias voltage, showing the interesting competition behaviors. The BBP with interesting electronic and transport properties are expected to have potential applications in nanoelectronics.

Acknowledgments

This work was supported by Hong Kong Scholars Program No. XJ2016007and XJ2018051, project National Natural Science Foundation of China under Grants No. 11704291, No.11647047 and No. 11704292, and HK PolyU under Grant No. G-YBHY, and Foundation for University Key Teachers from the WUST of No. 2017xz024.

References

[1] Novoselov KS, Geim AK, Morozov SV, Jiang D, Zhang Y, Dubonos SV, Grigorieva IV and Firsov AA 2004 Electric field effect in atomically thin carbon films science 306 666-669

[2] Novoselov K, Jiang D, Schedin F, Booth T, Khotkevich V, Morozov S and Geim A 2005 Two-dimensional atomic crystals. Proceedings of the National Academy of Sciences 102 10451-10453.

[3] Li L, Yu Y, Ye GJ, Ge Q, Ou X, Wu H, Feng D, Chen XH and Zhang Y 2014 Black phosphorus field-effect transistors Nature nanotechnology 9 372

[4] Xia F, Wang H and Jia Y 2014 Rediscovering black phosphorus as an anisotropic layered material for optoelectronics and electronics Nature communications 2014 5 4458

[5] Liu H, Neal AT, Zhu Z, Luo Z, Xu X, Tománek D and Ye PD 2014 Phosphorene: An unexplored 2d semiconductor with a high hole mobility ACS nano 8 4033-4041

[6] Tran V, Soklaski R, Liang Y and Yang L 2014 Layer-controlled band gap and anisotropic excitons in few-layer black phosphorus Physical Review B 89 235319

[7] Zhu Z and Tománek D 2014 Semiconducting layered blue phosphorus: A computational study Physical review letters 112 176802

[8] Guan J, Zhu Z and Tománek D 2014 Phase coexistence and metal-insulator transition in few-layer phosphorene: A computational study. Physical review letters 113 046804

[9] Zhang JL, Zhao S, Han C, Wang Z, Zhong S, Sun S, Guo R, Zhou X, Gu CD and Yuan KD 2016 Epitaxial growth of single layer blue phosphorus: A new phase of two-dimensional phosphorus Nano letters 16 4903-4908

[10] Xu J-P, Zhang J-Q, Tian H, Xu H, Ho W and Xie M 2017 One-dimensional phosphorus chain and two-dimensional blue phosphorene grown on au (111) by molecular-beam epitaxy Physical Review Materials 1 061002

[11] Geim A, Ak geim and ks novoselov 2007 The rise of graphene Nat. Mater. 6, 183

[12] Radisavljevic B, Radenovic A, Brivio J, Giacometti iV and Kis A 2011 Single-layer mos 2 transistors. Nature nanotechnology 6 147

[13] Xie J, Si M, Yang D, Zhang Z and Xue D 2014 A theoretical study of blue phosphorene nanoribbons based on first-principles calculations. Journal of Applied Physics 116 073704

[14] Hohenberg P and Kohn W 1964 Inhomogeneous electron gas. Physical review 136 B864

[15] Kohn W and Sham lj 1965 Self-consistent equations including exchange and correlation effects phys. Rev. 140 A1133

[16] Taylor J, Guo H and Wang J 2001 Ab initio modeling of quantum transport properties of molecular electronic devices Physical Review B 63 245407

[17] Brandbyge M, Mozos J-L, Ordejón P, Taylor J and Stokbro K 2002 Density-functional method for nonequilibrium electron transport Physical Review B 65 165401

[18] Soler JM, Artacho E, Gale JD, García A, Junquera J, Ordejón P and Sánchez-Portal D 2002 The siesta method for ab initio order-n materials simulation Journal of Physics: Condensed Matter 14 2745

[19] Ghosh B, Nahas S, Bhowmick S and Agarwal A 2005 Electric field induced gap modification in ultrathin blue phosphorus Physical Review B 91 115433

[20] Zeng M, Shen L, Zhou M, Zhang C and Feng Y 2011 Graphene-based bipolar spin diode and spin transistor: Rectification and amplification of spin-polarized current Physical Review B 83 115427

[21] Li Z, Qian H, Wu J, Gu B-L and Duan W 2008 Role of symmetry in the transport properties of graphene nanoribbons under bias Physical review letters 100 206802

Figure caption

Figure 1

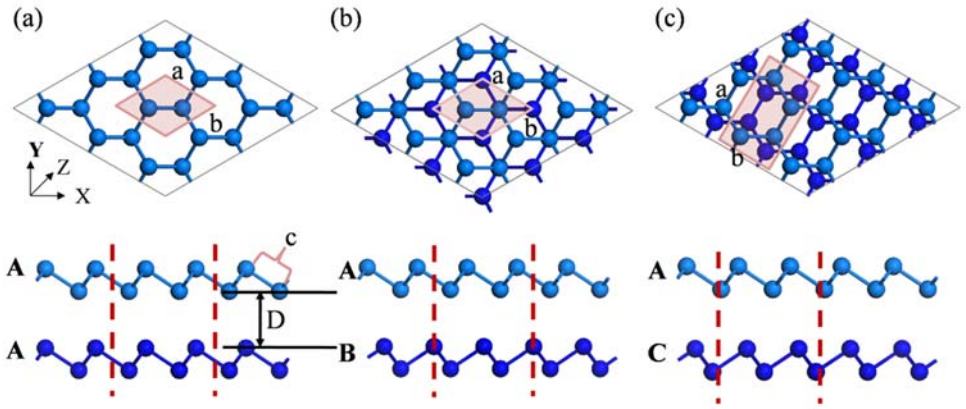

FIG. 1 Top and side views of three kinds (a) AA-, (b) AB- and (c) AC stackings constructions bilayer blue phosphorene

Figure 2

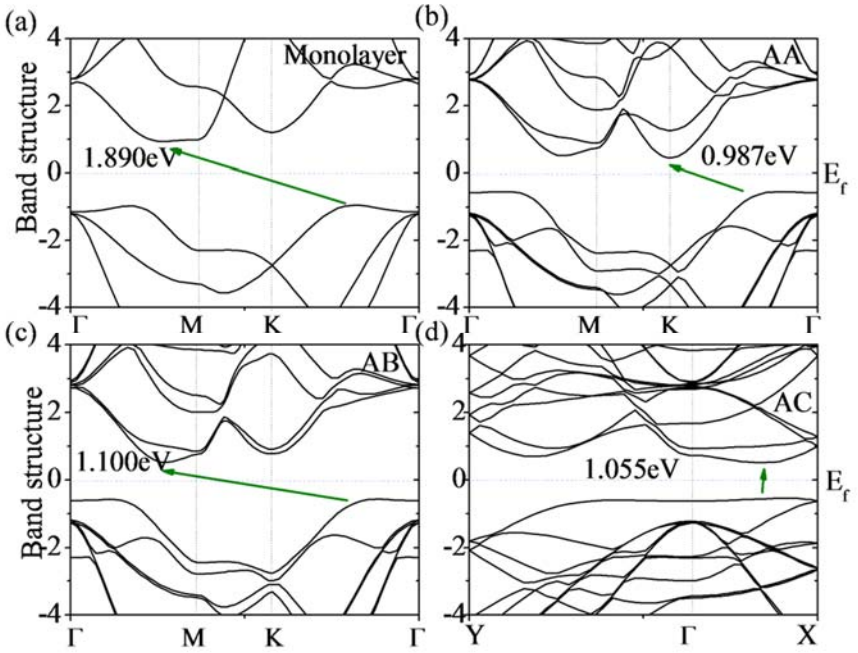

FIG. 2 The band structure of the monolayer and bilayer blue phosphorus.

Figure 3

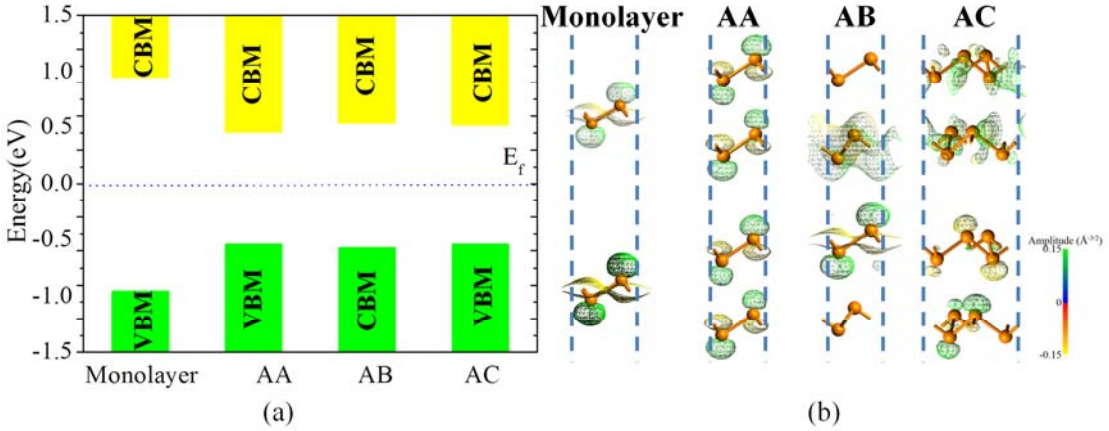

FIG. 3 Energy levels of conduction band offset (CBM), and valence band offset (VBM) of monolayer and bilayer BlueP. (c) Isosurface plot of orbitals from molecular projected self-consistent Hamiltonian (MPSH) of BBP. The crystalline orbitals of the monolayer and bilayer BlueP calculated for the Γ point corresponding to CBM and VBM. The isovalue is 0.15Å$^{-3/2}$.

Figure 4

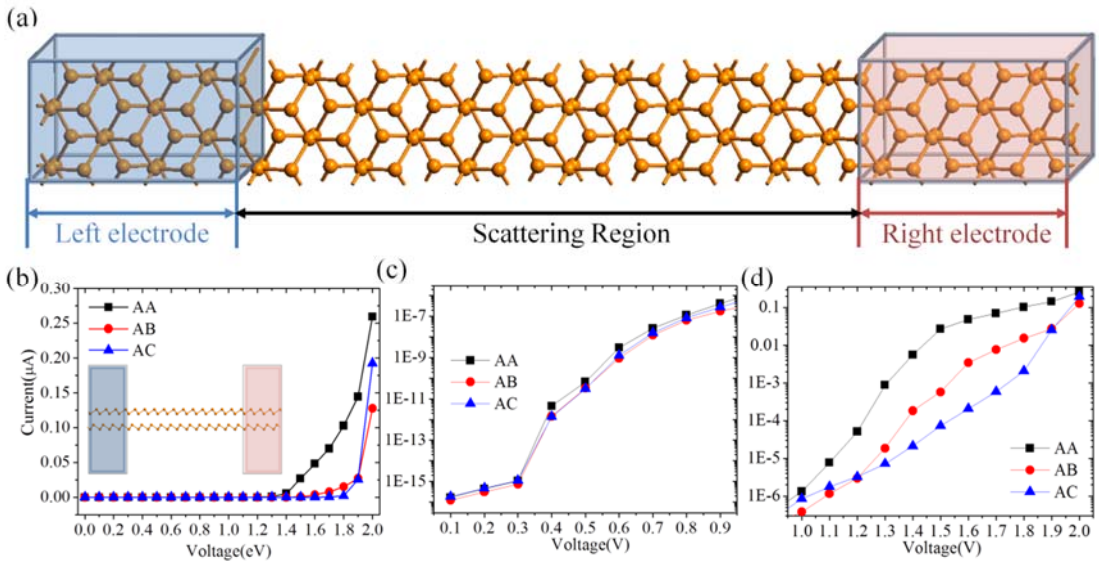

FIG. 4 (a) Structures of AB stacking bilayer BlueP schematic device model of two probe system. The blue frame indicates the semi-infinite left leads while the pink one indicates the semi-infinite right leads. (b)-(d)The current-voltage curve.

Figure 5

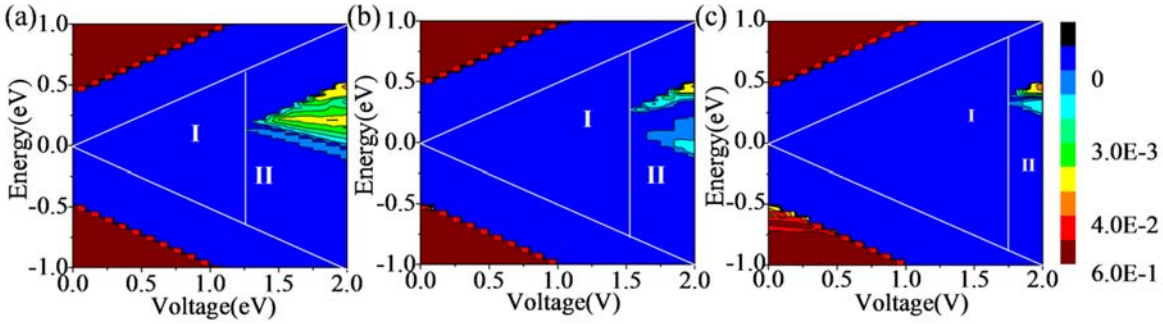

FIG. 5 The transmission coeffients as a function of electron energy E and bias voltage for (a) AA-, (b) AB- and (c) AC stacking bilayer BlueP. Note that region I and region II are bias windows.

Figure 6

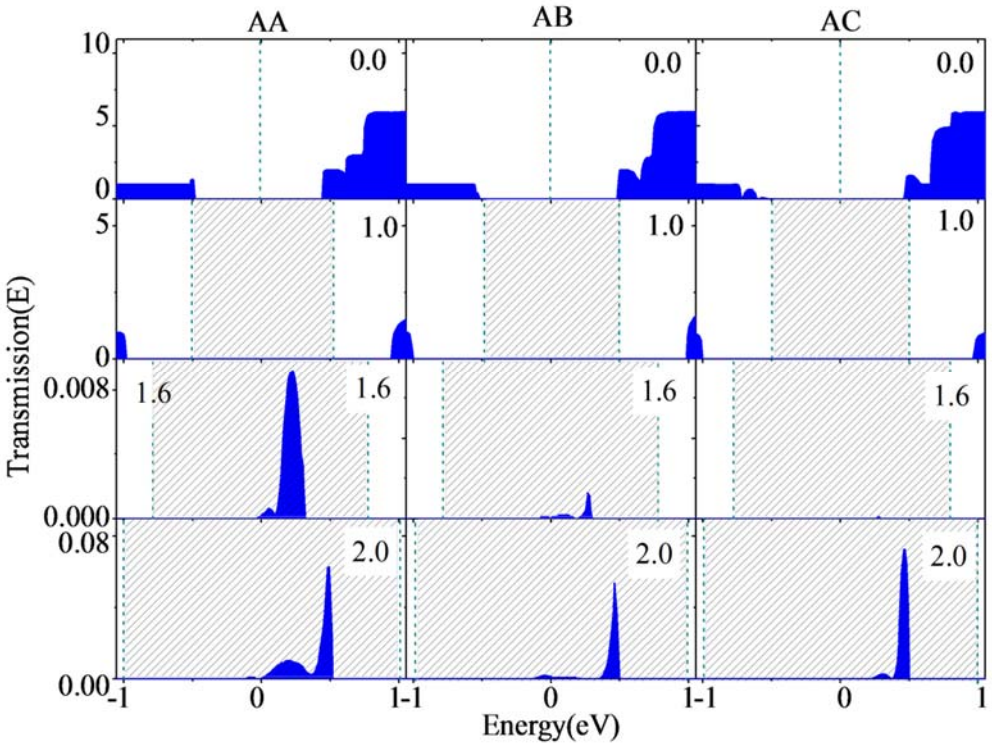

FIG. 6 The transmission spectra of bilayer BlueP at bias voltage 0.0V, 1.0V, 1.6V and 2.0V.

Figure 7

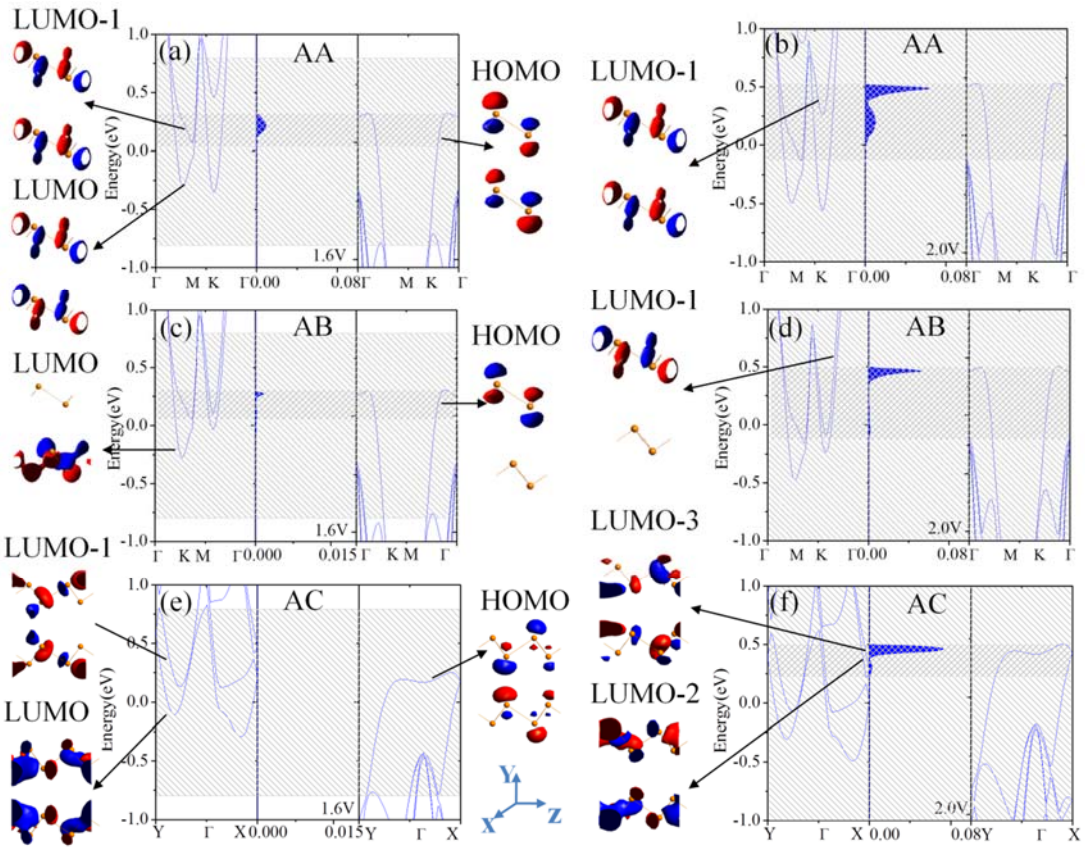

FIG. 7 The band structures of left electrode (left panel) and right electrode (right panel), along with the transmission spectra (middle panel), for a bias of 1.6 V and 2.0V, separately. The light-grey shadow represents the bias window and the dark-grey shadow represents the efficacious transmission channel. The corresponding electronic orbitals are also shown.

Table caption

Table 1 Equilibrium structure parameters of the monolayer and bilayer blue phosphorus.

Type	a(Å)	b(Å)	c(Å)	D(Å)	E_b(eV)	E_g(eV)	CBM(eV)	VBM(eV)
Monolayer	3.32	3.32	2.2912		0	1.890	0.938	0.955
AA	3.267	3.267	2.2711	3.214	0.230	0.987	0.442	0.545
AB	3.267	3.267	2.2705	3.248	0.231	1.100	0.524	0.576
AC	3.267	5.659	2.2709	3.262	0.210	1.055	0.509	0.546